Article

Synthesis of High-Quality Two-Dimensional V_2C MXene for Supercapacitor Application [†]

Wangsheng Ai, Chunfei Zhang, Lan Xia, He Miao (ORCID) **and Jinliang Yuan** *(ORCID)

Faculty of Maritime and Transportation, Ningbo University, Ningbo 315832, China;
1911084036@nbu.edu.cn (W.A.); zhangchunfei@nbu.edu.cn (C.Z.); xialan@nbu.edu.cn (L.X.);
miaohe@nbu.edu.cn (H.M.)
* Correspondence: yuanjinliang@nbu.edu.cn; Tel.: +86-0547-87609795
† This paper is an extended version of our paper in the 13th International Conference on Applied Energy (ICAE2021), Digital Meeting, 29 November–5 December 2021.

Abstract: Two-dimensional (2D) V_2C MXene has fascinating potential for use as electrodes in high-energy-density supercapacitors because of its excellent electrical conductivity and large specific surface area. However, it is not feasible to synthesize V_2C by etching vanadium carbon aluminide (V_2AlC) with hydrofluoric acid, which is commonly used for preparing other MXenes. In this work, a modified method is developed for synthesizing high-quality 2D V_2C. A mixture of sodium fluoride (NaF) and hydrochloric acid (HCl) was used as the etching agent, where V_2AlC can be gently etched by a hydrothermal reactor-assisted method. As electrode materials for supercapacitors, V_2C shows the characteristics of electric double layer capacitance. The electrochemical results show high specific capacitance (223.5 F/g in 1 M Na_2SO_4 at a current density of 100 mA/g) and good cycling stability (the capacitance retention rate can be maintained at 94.7% after 5000 cycles). This work provides a new method for the synthesis of high-quality V_2C for application in related fields.

Keywords: V_2C; supercapacitors; MXene; specific capacitance; cycling stability

1. Introduction

Supercapacitors are an internationally recognized, new energy storage device between secondary batteries and ordinary capacitors, because they have higher specific power, longer cycle life, and faster response than secondary batteries [1–3]. Thus, supercapacitors have attracted extensive consideration for their superior energy storage efficiency. Depending on the different energy storage mechanisms, capacitors generally can be classified into two types: electric double-layer capacitors (EDLCs) and pseudocapacitors [4,5]. Porous carbon materials and most transition metal oxides/sulfides are common materials for the capacitors, which show the electric double-layer capacitance and pseudocapacitance [6–11], respectively. Although carbon materials have a large specific surface area (about 1000–2000 m^2/g), their conductivity is discounted because of highly porous structures that affect their performance as EDLCs electrode materials [12]. Transition metal oxides/sulfides have much higher capacitance than carbon materials, but the disadvantages of narrow voltage window, poor cycle performance, and low electrical conductivity are still large challenges [13]. Therefore, development of new electrode materials to meet typical merits of the supercapacitors is necessary.

In recent years, MXenes, as a new family of two-dimensional layered materials, have been widely studied as electrode materials for the supercapacitors. MXenes have been highly anticipated in the energy storage field since they were first reported by Barsoum and Gogotsi in 2011 [14]. As reported elsewhere, wet synthesis is the main preparation method for MXenes. The common method employed is hydrofluoric acid etching, and the A phase is selectively etched away from the $M_{n+1}AX_n$ compound. In the process of etching, the surface of MXenes is generally covered with oxygen (-O), hydroxyl (-OH), and fluorine (-F)

groups; MXenes are also named $M_{n+1}X_nT_x$, while T_x represents the surface chemical groups (-O, -OH, and -F) on MXenes. Gogotsi's team found that MXenes have high electrical conductivity, tunable surface (functional group) structure, surface hydrophilicity, and great stability [15]. Many research reports have demonstrated the promising application prospects of MXenes as candidate materials for the preparation of secondary batteries and supercapacitor electrodes [16–18]. However, Ti_3C_2 has been mostly studied in the MXenes family. There are only a few studies on V_4C_3 [19], Ti_2C [20], Nb_2C [21], Ta_3C_2 [22], Ta_2C [23], Ti_3C_2 [24], Hf_3C_2 [25], Zr_2C [26], Cr_2C [27], etc. Only limited research on V_2C has been performed recently [28–30] because the traditional method of using fluoride salt and hydrochloric acid as a wet-chemical etching solution cannot produce effective etching of V_2AlC, which also leads to the generation of impurity. Therefore, the more effective method should be developed to synthesize high-quality V_2C. The two different etching methods on the preparation of V_2C were investigated, and the electrochemical performance of V_2C prepared without hydrofluoric acid was also explored.

High-quality V_2C was successfully prepared by a modified methodology and is reported in this paper. The Al layer in the V_2AlC phase was stripped off by NaF/HCl solution in a hydrothermal reaction at high pressure and high temperature. The $Na_5Al_3F_{14}$ impurity generated in the reaction was removed in sequence by a rinse with Na_2CO_3 solution and diluted sulfuric acid. The synthesis conditions of V_2C were optimized and the electrochemical performance of V_2C as a supercapacitor electrode was studied. The as-prepared material shows the best performance with a specific capacitance of 556.7 F/g in 1 M Na_2SO_4 at a scan rate of 2 mV/s, which is much better than Ti_3C_2 (~100 F/g) [31]. The specific capacitance was 223.5 F/g at the current density of 100 mA/g, and the capacitance retention rate was 94.7% after 5000 cycles, indicating good cycling stability.

2. Materials and Preparation Methods

2.1. Materials

The chemical materials are shown in Table 1.

Table 1. Chemical materials.

Materials	Chemical Formula	Molecular Mass
Vanadium Carbide Aluminide	V_2AlC	140.8
Hydrochloric Acid	HCl	36.46
Sulfuric Acid	H_2SO_4	98.08
Sodium Fluoride	NaF	41.99
Potassium Hydroxide	KOH	56
Sodium Carbonate	Na_2CO_3	105.99
Polyvinylidene Fluoride	$-(C_2H_2F_2)_n-$	——
N-Methylpyrrolidone	C_5H_9NO	99.13

2.2. Synthesis of V_2C

V_2C was synthesized by using a mixture of HCl (Hangzhou ShuangLin Chemical Reagent Co., Ltd., Hangzhou, China) and NaF (Sinopharm Chemical Reagent Co., Ltd., Beijing, China) and selective etching of Al atoms from V_2AlC (11 Technology Co., Ltd., Jilin, China). The fabrication process is shown in Figure 1. In detail, 1 g of V_2AlC was placed in an etching solution consisting of 50 mL hydrochloric acid and 2 g sodium fluoride. This mixture was transferred to a 100 mL Teflon stainless-steel autoclave after 30 min, and then cooled to room temperature after 96 h [32–34]. The sediment in the stainless-steel autoclave was collected after centrifuging for 5 min (3500 rpm). The products were then washed with ample deionized water (until pH ≥ 6) and dried at 60 °C overnight in a vacuum oven. This product was recorded as V_2C-96. The product was collected and treated with Na_2CO_3 at 90 °C for 12 h, and washed with diluted sulfuric acid for 6 h to obtain multilayered V_2C. For comparison, the samples with 24, 48, 72, and 120 h reaction times were prepared by the same method, recorded separately as V_2C-24, V_2C-48, V_2C-72, and V_2C-120. Similarly, the

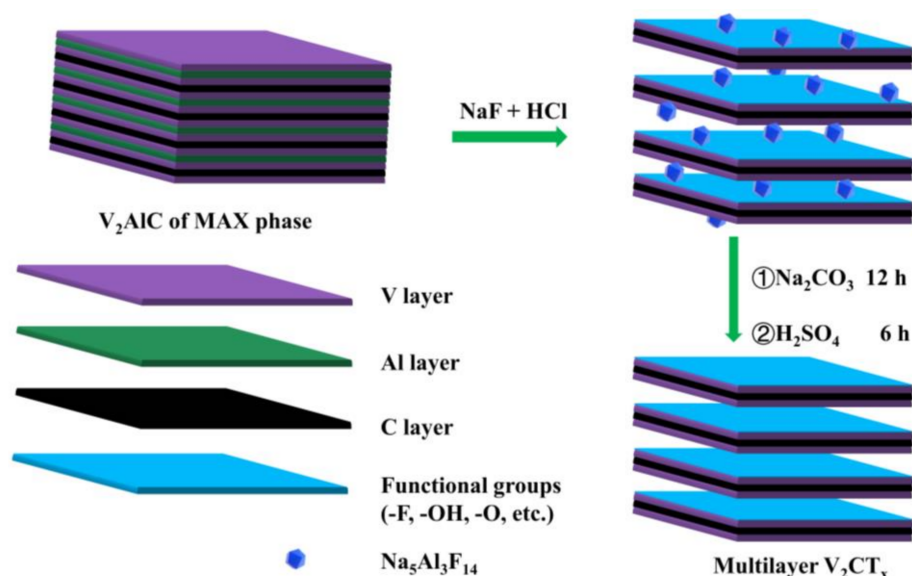samples were also prepared at different reaction temperatures of 50 and 70 °C, recorded separately as V_2C-50° and V_2C-70°.

Figure 1. Schematic diagram of V_2C synthesis process.

2.3. Preparation of the V_2C Flexible Electrodes

Carbon cloth was used as the current collector for the fabricated flexible electrodes. A certain mass of Polyvinylidene Fluoride (PVDF) was dispersed in 2 mL of *N*-Methylpyrrolidone (NMP) and stirred for 12 h. A certain mass of MXene and acetylene black was weighed in proportion and ground in a mortar for 10 to 15 min to obtain a well-mixed powder. The mass ratio of V_2C:PVDF:acetylene black is 8:1:1 [32]. Then, the well-mixed powder was put into the prepared PVDF solution and stirred for more than 12 h to make a homogeneous slurry, which was uniformly painted on a piece of carbon cloth (8 mm in radius, ~25 mg) with a mass loading of 1 mg/cm². The electrode sheet coated with the active material was placed in a vacuum oven at 60 °C to dry overnight.

2.4. Characterization and Electrochemical Analysis

Scanning electron microscopy (SEM, Hitachi S4800) and transmission electron microscopy (TEM, Talos-F200X) combined with energy dispersive X-ray (EDX) were used to analyze the surface morphologies, microstructures, and elements of the prepared samples in this work. The crystal structure was analyzed using X-ray diffraction (XRD D8 Advance, Bruker) conducted at 40 mA and 45 kV with Cu Kα radiation (λ = 0.15418 nm, 5° min^{-1}). X-ray photoelectron spectra (XPS) were acquired on a Scanning Auger XPS Thermo Scientific K-Alpha. The fitting of the XPS spectra was carried out using Avantage software.

In this work, the electrochemical testing of the V_2C as the supercapacitor electrodes were performed with a three-electrode system in CHI660E. For the three-electrode tests, the V_2C electrodes were employed as the working electrode, Ag/AgCl as the reference electrode, and a carbon rod as the counter electrode. The tests were carried out in 1 M Na_2SO_4, H_2SO_4, and KOH electrolytes. The supercapacitor was constructed by two MXene electrodes and a filter paper separator. The cyclic voltammetry (CV) tests were carried out with the potential window −0.4~0.4 V in the different electrolytes, 1 M Na_2SO_4, 1 M KOH, and 1 M H_2SO_4. The electrochemical tests, including CV, electrochemical impedance spectroscopy (EIS), and galvanostatic charge–discharge (GCD), were performed at room temperature (~25 °C). For the supercapacitor device that was prepared, the V_2C electrodes and separator (i.e., the cellulose paper) were soaked in 1 M Na_2SO_4 for 6 h, and then the symmetric cell was assembled in sequence with a V_2C electrode, a separator, and a V_2C electrode, which was then packaged and sealed with parafilm. The cycling stability

testing was performed on a multichannel battery testing system (LAND CT2001A) at room temperature. According to the result of the CV curves, the gravimetric capacitance of the electrode was calculated by using Formula (1) [11]:

$$C = \frac{\int I dV}{vm\Delta V} \tag{1}$$

where ΔV is the potential window, I is the applied current, v is the scan rate, and m is the mass of the active materials.

For the three-electrode system, the specific capacitance (C_A, F/g) was calculated using Formula (2), according to the GCD curves [35]:

$$C_A = (I \times \Delta t)/(m \times \Delta V) \tag{2}$$

where ΔV is the potential window, I is the discharge current, m is the mass of the active materials, and Δt is the discharge time.

The two-electrode device was assembled for energy density (E, Wh/kg), evaluated using Formula (3), while the specific capacitance for the two-electrode device was calculated by using Formula (4) [36,37].

$$E = 1/2\left(C_{device} \times \Delta V^2\right) \tag{3}$$

$$C_{device} = 4(I \times \Delta t)/(M \times \Delta V) \tag{4}$$

where ΔV is the potential window of the discharge process excluding the potential drop, Δt is the discharge time, I is the discharge current, M is the total mass of the two electrodes.

3. Results and Discussion

3.1. Material Characterization

As shown in Figure 2a, the original XRD spectra of V_2AlC shows typical characteristic peaks at $2\theta \approx 13.5°$ and $41.3°$, which belong to (002) and (103) crystal phases, respectively. It has been reported that the hydrofluoric acid etching is effective for the preparation of Ti_3AlC_2 but not for V_2AlC [14,24,38]. The sodium fluoride (NaF) and hydrochloric mixture is often used for V_2C preparation [39,40]. In order to obtain highly delaminated V_2C, a hydrothermal reactor was used to assist the etching reaction in this work, which can provide a high-pressure and temperature environment. V_2C was prepared with different reaction time (Figure 2b) and temperatures (Figure 2c) in the etching reactions, by which the temperature and time for the etching reactions were optimized. The XRD results are shown in Figure 2b,c. When the etching was performed at 90 °C, the typical (002) peak of V_2C shifted to 7.41° from 13.45° with increase in the reaction time. During the etching process, the interlayer space increased significantly; the intensity of (103) peak for V_2AlC greatly decreased, which implies that the Al layer in the MAX phase was etched away by the mixture of the fluorine salt and hydrochloric acid.

Therefore, 96 h are considered enough for the etching reactions. It was noticed that the byproducts of $Na_5Al_3F_{14}$ could be removed by Na_2CO_3 and the diluted sulfuric acid, as shown in Figure 2d. The etching experiments were also conducted under much lower temperatures, 50 and 70 °C. The XRD results show that the two characteristic peaks of the MAX phase for (002) and (103) did not change significantly at 50 °C. The characteristic diffraction peaks of the MAX phase decreased greatly when the temperature increased to 70 °C. If the temperature rises to 90 °C, the (002) peak shifts from 13.45° to 7.41°, and the (103) peak disappears, which indicates that 90 °C is considered as the optimal temperature (Figure 2c).
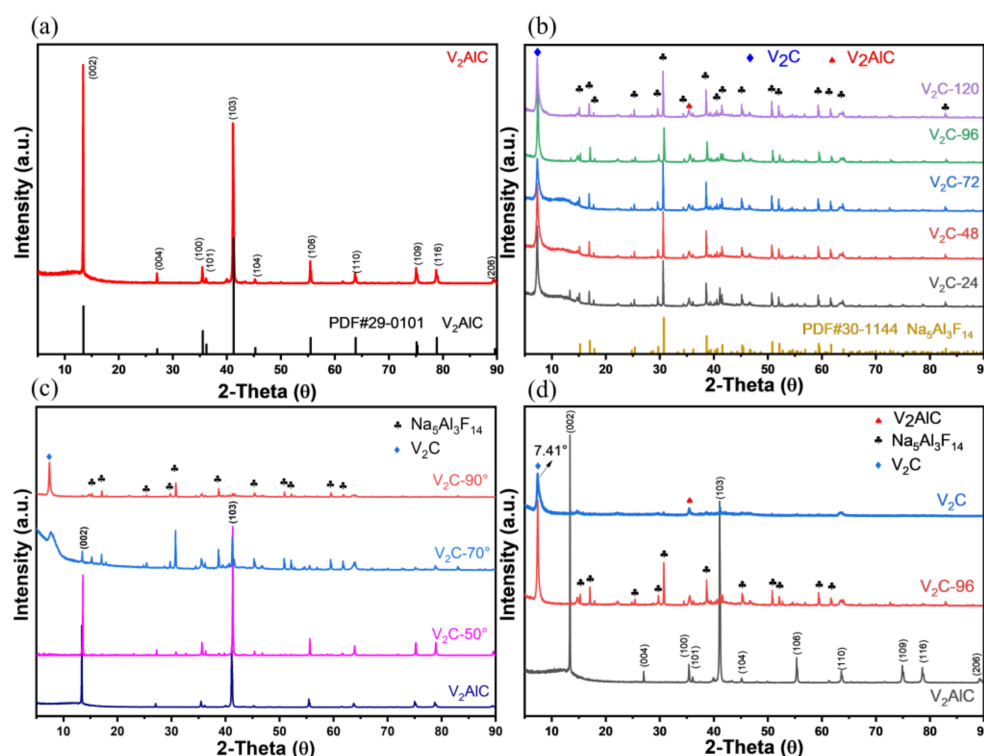
Figure 2. XRD spectra of (**a**) V₂AlC, (**b**) samples with different reaction time, (**c**) samples with different reaction temperatures, (**d**) V₂C before and after purification.

Figure 3 shows the SEM images of the samples synthesized with different reaction time and temperatures. It can be seen that V_2AlC has a dense structure without any delamination, as shown in Figure 3a. Figure 3b–f shows the samples for different reaction times of 24, 48, 72, 96, and 120 h, respectively. Significantly, increasingly more MAX can be fully etched with prolongation of the etching time. The byproduct of $Na_5Al_3F_{14}$, also shown in Figure 3i, could be removed by sodium carbonate and dilute sulfuric acid. Note that the Al layer in V_2AlC was almost fully removed after 96 h, and a typical 2D layered "accordion" morphology is observed. As shown in Figure 3g,h, the V_2AlC could not be etched at 50 °C, while a large number of the V_2C nanosheets were observed at 70 °C. The Al atoms were almost completely etched out when the temperature rose to 90 °C. The SEM images and XRD results indicate that 90 °C and 96 h are the optimal reaction conditions for V_2C preparation. Therefore, the V_2C-96 samples after purification were used for the following characterizations and electrochemical performance evaluation.

Figure 4 shows the TEM and EDX image of V_2CT_x. It can be found that the d-spacing value is 0.95 nm from the pattern obtained (Figure 4a), which is consistent with that in the previous study [41,42]. Figure 4b shows that a large number of V_2C nanosheets are connected together, which indicates that the A layer in the MAX phase is basically etched. The EDX mapping images clearly show the V, C, Al, and F elements, in which Al may come from a small amount of MAX residue. The contents of V, Al, C, and F elements are shown in Table 2; it was found that the atomic ratio of V:Al is 57.93:1.01, which indicates that more than 95% of V_2AlC was converted into V_2C.
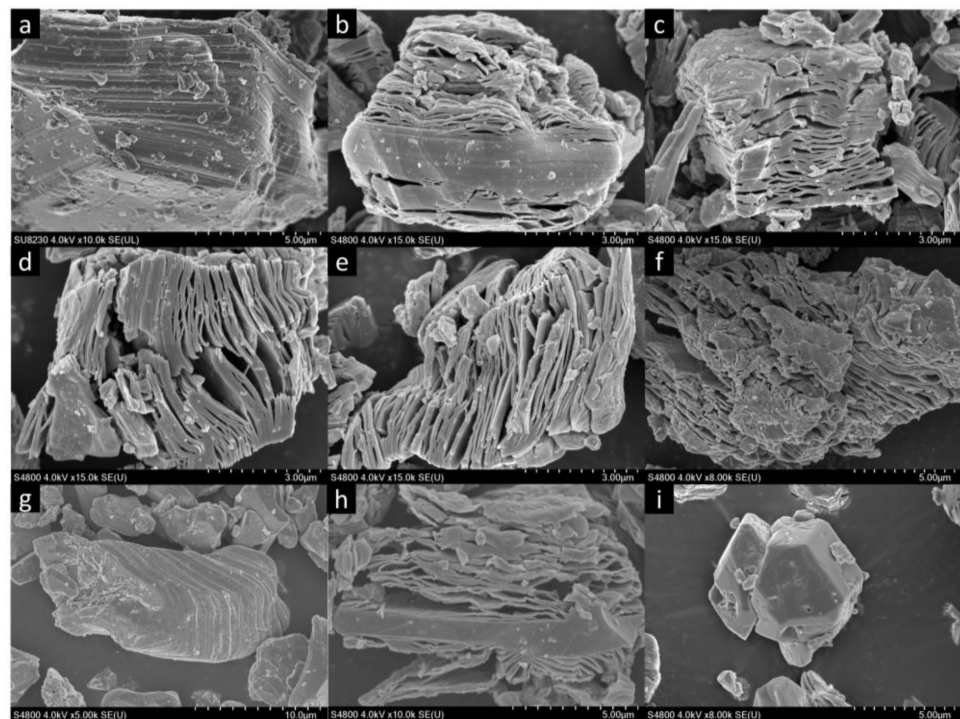
Figure 3. (**a**) SEM image of V_2AlC, (**b–f**) SEM images of V_2C-24, V_2C-48, V_2C-72, V_2C-96, and V_2C-120, respectively. (**g**) SEM image of V_2C-50 °C, (**h**) SEM image of V_2C-70 °C, (**i**) SEM image of $Na_5Al_3F_{14}$.
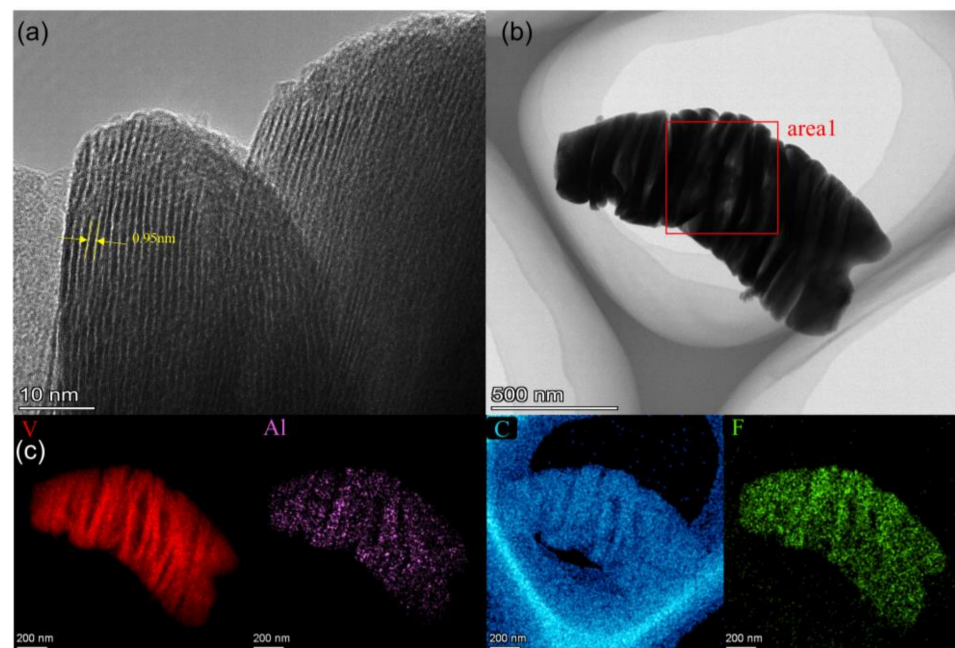

Figure 4. (**a**) HR–TEM and (**b**) TEM images of V_2C, (**c**) TEM–EDX elemental mapping images of V_2C.

Table 2. The element contents in the material (area 1).

Element	Atomic Fraction (%)	Mass Fraction (%)
C	29.82	10.09
F	11.24	6.01
Al	1.01	0.77
V	57.93	83.13

The elemental composition and termination species of the MAX phase V_2AlC and the corresponding MXene V_2C were measured by the X-ray photoelectron spectroscopy (XPS). Almost complete disappearance of the Al 2p and Al 2s peaks in the XPS spectrum proves that the Al layer in the MAX phase was successfully etched away (see Figure 5a) [19]. As shown in Figure 5b, the peaks at 513.6 and 521.2 eV correspond to the V-C bond, and the peaks at 516.5 and 524.1 eV correspond to the V-O bond in V_2C. The spectrum in the O 1s region (Figure 5c) for the V_2CT_x is well fitted by V-O, O-H, and the adsorbed H_2O, while the corresponding binding energy peaks are located at 530.3, 531.8, and 533.6 eV [43], respectively. From the peak fitting of C 1s (Figure 5d), the peaks at 282.2, 284.6, 286.2, and 288.9 eV can be assigned to the C-V, C-C, C-O, and O-C=O bonds, respectively, which are consistent with those reported elsewhere [18]. From the XPS spectra, it is confirmed that the V_2C prepared by the fluoride salt method, similar to other MXenes, also has functional groups such as -F, -O, and -OH. There is also H_2O adsorbed on the surface of V_2C [43,44].
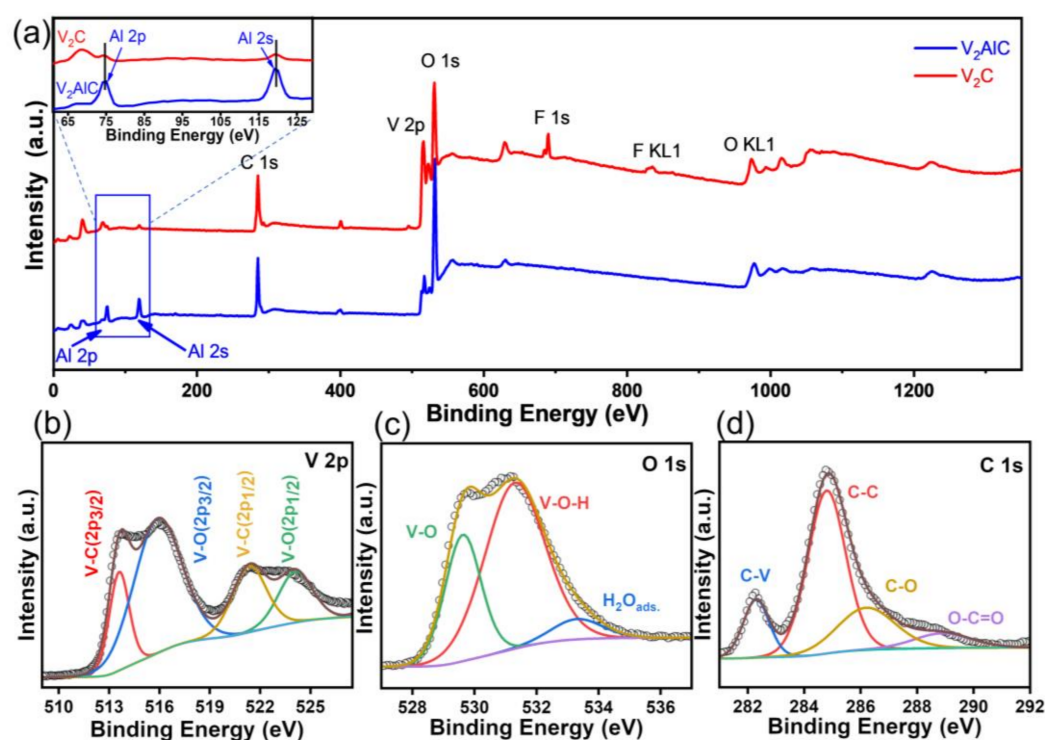

Figure 5. (**a**) The XPS spectra of V_2AlC and V_2C, (**b**) V 2p, (**c**) O 1s, (**d**) C 1s.

3.2. Electrochemical Performance of Flexible V_2C Electrodes

The flexible V_2C electrode sheets were prepared for the electrochemical performance evaluated in 1 M H_2SO_4, Na_2SO_4, and KOH solutions using a three-electrode system on CHI660E. Figure 6a–c shows the characteristic CV curves for different scan rates of 2, 5, 10, 20, 50, and 100 mV/s with the potential window of −0.4~0.4 V in 1 M H_2SO_4, KOH, and Na_2SO_4, respectively. At the scan rate of 2 mV/s, the specific capacitance is 113.4 F/g, 96.4 F/g, and 556.7 F/g for the acid electrolyte, alkaline electrolyte, and neutral electrolyte, respectively. At a higher scan rate of 100 mV/s, the specific capacitance of V_2C can still be maintained at 194.6 F/g in 1 M Na_2SO_4 electrolyte. The specific capacitances of the V_2C electrodes decrease gradually with increasing scan rates (Figure 6d). Interestingly, the V_2C materials show much higher specific capacitance in Na_2SO_4 than in H_2SO_4 or KOH electrolytes. Compared with K^+, Na^+ has a much smaller hydrated ionic radius, which can be inserted more easily into the interlamination of V_2C layers. Moreover, the cation concentration in Na_2SO_4 is much better than that in KOH, and thus the former has higher ionic conductivity. The reason is because a large number of F terminal groups on the surface of V_2C may form hydrogen bonds with H in H_2SO_4, which greatly restricts the movement

of H^+ and leads to the worse performance. Moreover, note that the as-prepared electrodes show much higher specific capacitance in Na_2SO_4 electrolyte compared with that of the V_2C samples synthesized by other methods (Table 3), indicating an improved performance is obtained for the as-synthesized V_2C samples.
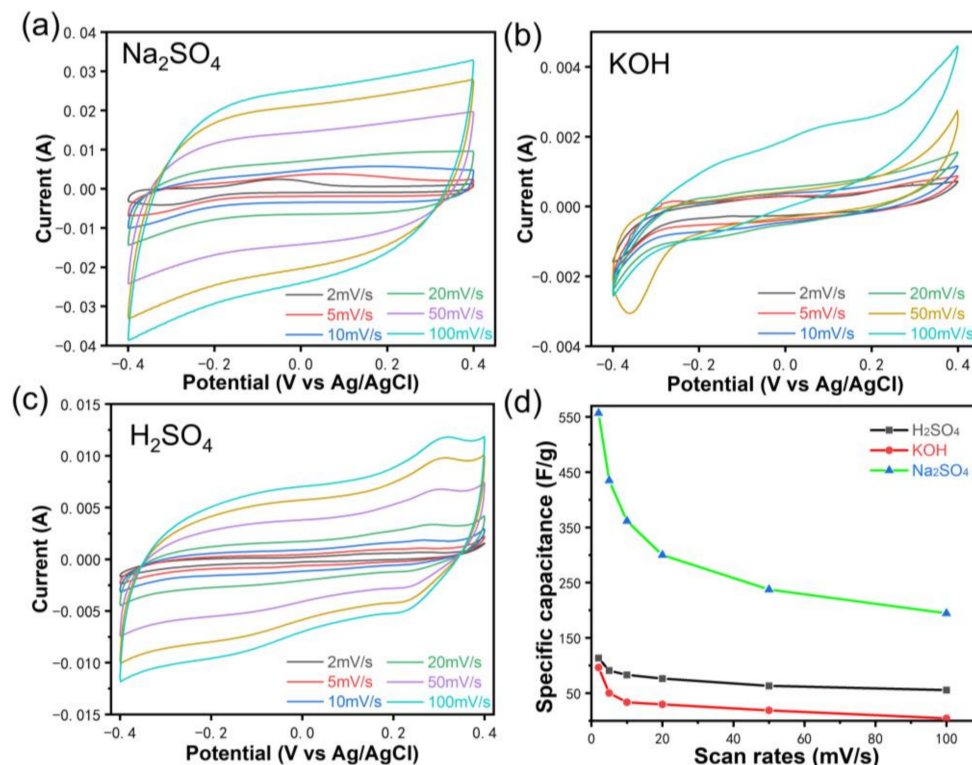

Figure 6. Cyclic voltammograms of V_2C electrodes at different scan rates (**a**) 1 M Na_2SO_4 electrolyte, (**b**) 1 M KOH electrolyte, (**c**) 1 M H_2SO_4 electrolyte, (**d**) specific capacitance based on the CV results.

Table 3. The specific capacitance of different V_2C electrodes.

Electrode Materials	Specific Capacitance (F/g)	Scan Rates (mV/s)	Electrolyte	References
V_2C (NaF + HCl)	556.7	2	Na_2SO_4	This work
V_2C (NaF + HCl)	113.4	2	H_2SO_4	This work
V_2C (NaF + HCl)	96.4	2	KOH	This work
V_2C (NaF + HCl)	361	10	Na_2SO_4	This work
V_2C (KF + HCl)	164	2	Na_2SO_4	[42]
V_2C (49 wt% HF)	225	2	Mg_2SO_4	[45]
V_2C (49 wt% HF)	487	2	H_2SO_4	[45]
V_2C (50 wt% HF)	100	0.2	$NaPF_6$	[46]
V_2C (50 wt% HF)	120	10	Na_2SO_4	[47]

Figure 7a,b shows the GCD curves and specific capacitances of V_2C electrodes at different current densities in 1 M Na_2SO_4 electrolyte. The voltage drops of these electrodes are not observed, indicating that the prepared electrodes have good electrical conductivity and less polarization. The single electrode specific capacitance of the supercapacitor is as high as 223.5 F/g, achieved at a current density of 100 mA/g. Figure 7c shows the impedance of V_2C and carbon cloth electrodes in 1 M Na_2SO_4 electrolyte. It can be seen that the solution resistance (R_s) of 1.982 ohm (including the resistances of the electrode components) for the carbon cloth electrode is higher than that of the V_2C electrode (1.175 ohm), as shown in the magnified area in Figure 7d, which may result from the high hydrophobic surface area of the carbon cloth in the aqueous electrolyte. However, also note that the V_2C electrode shows a very small arc in the high frequency part, indicating

that the charge transfer resistance is small. Therefore, the EIS results further confirm that the as-prepared V_2C electrodes have good electrical conductivity. Moreover, the cycling performance of the electrodes was also studied. Note that the capacitance decreased quickly during the initial 100 cycles and then became steady, which may ascribe to a small number of V_2C nanosheets falling off from the carbon cloth (Figure 7e). After the performance testing of 5000 cycles, a high capacitance retention rate up to 94.7% and an energy density of 9.3 Wh/kg for the device were obtained, indicating that excellent cycling stability was achieved for the flexible electrodes, which is comparable to that of $Ti_3C_2T_x$ MXene and $Ti_3C_2T_x$/RGO reported elsewhere [48].
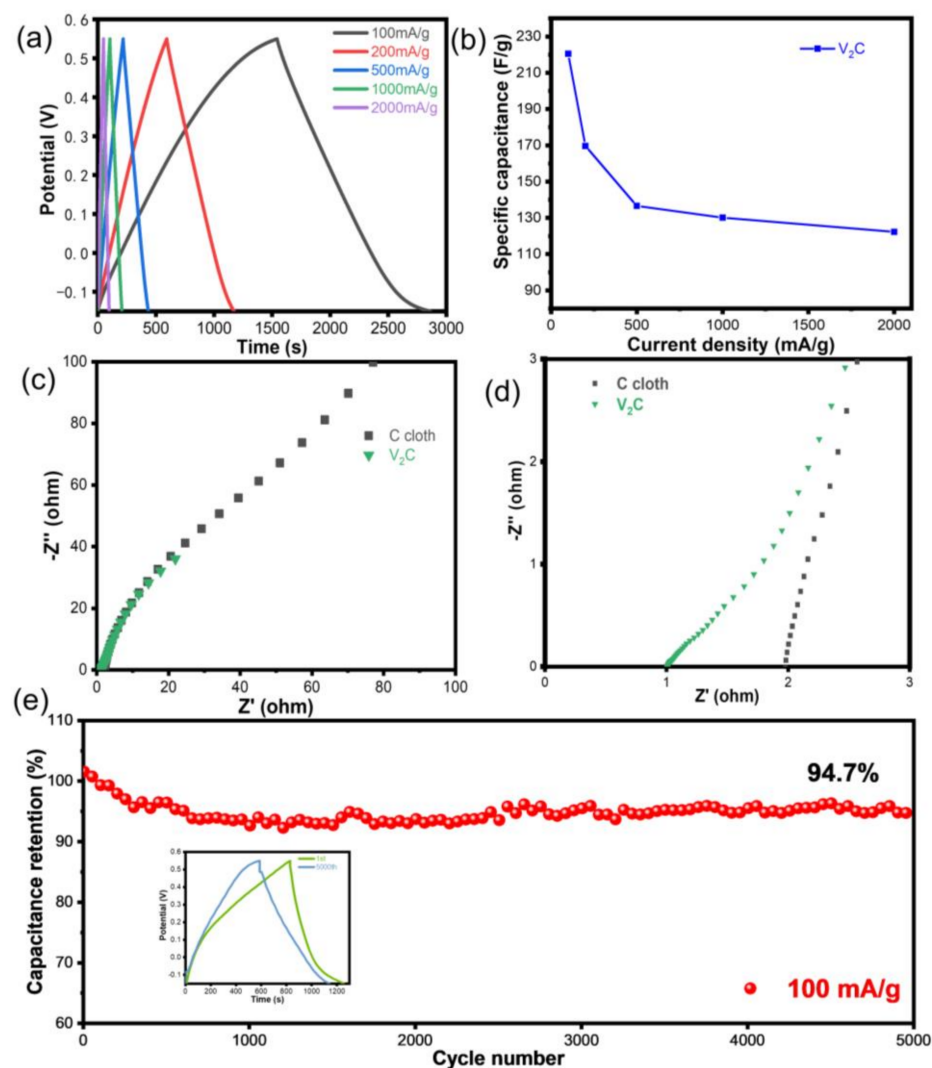

Figure 7. (**a**) GCD curves of V_2C at different current densities in 1 M Na_2SO_4, (**b**) specific capacitance at different current densities, (**c**) Nyquist plots of V_2C and carbon cloth, (**d**) magnified image of the Nyquist plots in the high frequency part, (**e**) cycling performance of V_2C evaluated at 100 mA/g.

4. Conclusions

The new method for synthesizing 2D V_2C MXene was developed to synthesize high-quality V_2C with good electrochemical performance as supercapacitor electrodes. The V_2C obtained was synthesized by a hydrothermal reactor-assisted etching method followed by an impurity removal process, and the synthesis conditions were optimized. The maximum specific capacitance of 223.5 F/g was obtained in 1 M Na_2SO_4. At a current density of 100 mA/g, the capacitance retention rate of 94.7% was obtained after 5000-cycle testing. The excellent electrochemical performance of the as-prepared V_2C MXene is attributed

to its high conductivity and 2D nanosheet structure with a high specific surface area, which offers additional options for the development of high-capacity and high-stability MXene-based supercapacitors.

References

1. Wang, G.; Zhang, L.; Zhang, J. A review of electrode materials for electrochemical supercapacitors. *Chem. Soc. Rev.* **2012**, *41*, 797–828. [CrossRef] [PubMed]
2. Yu, M.; Zhai, T.; Lu, X.; Chen, X.; Xie, S.; Li, W.; Liang, C.; Zhao, W.; Zhang, L.; Tong, Y. Manganese dioxide nanorod arrays on carbon fabric for flexible solid-state supercapacitors. *J. Power Sources* **2013**, *239*, 64–71. [CrossRef]
3. Liu, L.; Niu, Z.; Chen, J. Unconventional supercapacitors from nanocarbon-based electrode materials to device configurations. *Chem. Soc. Rev.* **2016**, *45*, 4340–4363. [CrossRef] [PubMed]
4. Simon, P.; Gogotsi, Y. Materials for electrochemical capacitors. *Nat. Mater.* **2008**, *7*, 845–854. [CrossRef]
5. Zhong, C.; Deng, Y.; Hu, W.; Qiao, J.; Zhang, L.; Zhang, J. A review of electrolyte materials and compositions for electrochemical supercapacitors. *Chem. Soc. Rev.* **2015**, *44*, 7484–7539. [CrossRef]
6. Sathiya, M.; Prakash, A.S.; Ramesha, K.; Tarascon, J.M.; Shukla, A.K. V_2O_5-anchored carbon nanotubes for enhanced electrochemical energy storage. *J. Am. Chem. Soc.* **2011**, *133*, 16291–16299. [CrossRef]
7. Zhai, T.; Xie, S.; Yu, M.; Fang, P.; Liang, C.; Lu, X.; Tong, Y. Oxygen vacancies enhancing capacitive properties of MnO_2 nanorods for wearable asymmetric supercapacitors. *Nano Energy* **2014**, *8*, 255–263. [CrossRef]
8. Lin, J.; Jia, H.; Liang, H.; Chen, S.; Cai, Y.; Qi, J.; Qu, C.; Cao, J.; Fei, W.; Feng, J. In Situ Synthesis of Vertical Standing Nanosized NiO Encapsulated in Graphene as Electrodes for High-Performance Supercapacitors. *Adv. Sci.* **2018**, *5*, 1700687. [CrossRef]
9. Liu, J.; Jiang, J.; Cheng, C.; Li, H.; Zhang, J.; Gong, H.; Fan, H.J. Co_3O_4 Nanowire@MnO_2 ultrathin nanosheet core/shell arrays: A new class of high-performance pseudocapacitive materials. *Adv. Mater.* **2011**, *23*, 2076–2081. [CrossRef]
10. Jiang, Q.; Kurra, N.; Alhabeb, M.; Gogotsi, Y.; Alshareef, H.N. All Pseudocapacitive MXene-RuO_2 Asymmetric Supercapacitors. *Adv. Energy Mater.* **2018**, *8*, 1703043. [CrossRef]
11. Zhang, L.L.; Zhao, X.S. Carbon-based materials as supercapacitor electrodes. *Chem. Soc. Rev.* **2009**, *38*, 2520–2531. [CrossRef] [PubMed]
12. Yu, D.; Goh, K.; Wang, H.; Wei, L.; Jiang, W.; Zhang, Q.; Dai, L.; Chen, Y. Scalable synthesis of hierarchically structured carbon nanotube–graphene fibres for capacitive energy storage. *Nat. Nanotechnol.* **2014**, *9*, 555–562. [CrossRef] [PubMed]
13. Wu, J.; Gao, X.; Yu, H.; Ding, T.; Yan, Y.; Yao, B.; Yao, X.; Chen, D.; Liu, M.; Huang, L. A Scalable Free-Standing V_2O_5/CNT Film Electrode for Supercapacitors with a Wide Operation Voltage (1.6 V) in an Aqueous Electrolyte. *Adv. Funct. Mater.* **2016**, *26*, 6114–6120. [CrossRef]
14. Naguib, M.; Kurtoglu, M.; Presser, V.; Lu, J.; Niu, J.; Heon, M.; Hultman, L.; Gogotsi, Y.; Barsoum, M.W. Two-dimensional nanocrystals produced by exfoliation of Ti_3AlC_2. *Adv. Mater.* **2011**, *23*, 4248–4253. [CrossRef]
15. Niu, S.; Wang, Z.; Yu, M.; Yu, M.; Xiu, L.; Wang, S.; Wu, X.; Qiu, J. MXene-Based Electrode with Enhanced Pseudocapacitance and Volumetric Capacity for Power-Type and Ultra-Long Life Lithium Storage. *ACS Nano* **2018**, *12*, 3928–3937. [CrossRef]
16. Luo, J.; Tao, X.; Zhang, J.; Xia, Y.; Huang, H.; Zhang, L.; Gan, Y.; Liang, C.; Zhang, W. Sn^{4+} Ion Decorated Highly Conductive Ti_3C_2 MXene: Promising Lithium-Ion Anodes with Enhanced Volumetric Capacity and Cyclic Performance. *ACS Nano* **2016**, *10*, 2491–2499. [CrossRef]
17. Hu, L.; Wu, L.; Liao, M.; Fang, X. High-performance $NiCo_2O_4$ nanofilm photodetectors fabricated by an interfacial self-assembly strategy. *Adv. Mater.* **2011**, *23*, 1988–1992. [CrossRef]
18. Rakhi, R.B.; Ahmed, B.; Hedhili, M.N.; Anjum, D.H.; Alshareef, H.N. Effect of Postetch Annealing Gas Composition on the Structural and Electrochemical Properties of Ti_2CT_x MXene Electrodes for Supercapacitor Applications. *Chem. Mater.* **2015**, *27*, 5314–5323. [CrossRef]
19. Wang, X.; Lin, S.; Tong, H.; Huang, Y.; Tong, P.; Zhao, B.; Dai, J.; Liang, C.; Wang, H.; Zhu, X.; et al. Two-dimensional V_4C_3 MXene as high performance electrode materials for supercapacitors. *Electrochim. Acta* **2019**, *307*, 414–421. [CrossRef]

20. Ahmed, B.; Anjum, D.H.; Hedhili, M.N.; Gogotsi, Y.; Alshareef, H.N. H_2O_2 assisted room temperature oxidation of Ti_2C MXene for Li-ion battery anodes. *Nanoscale* **2016**, *8*, 7580–7587. [CrossRef]
21. Mashtalir, O.; Lukatskaya, M.R.; Zhao, M.Q.; Barsoum, M.W.; Gogotsi, Y. Amine-Assisted Delamination of Nb_2C MXene for Li-Ion Energy Storage Devices. *Adv. Mater.* **2015**, *27*, 3501–3506. [CrossRef]
22. Wang, S.; Guan, C.; Zhao, Z.; Wang, R.; Tian, Y.; Du, Y. Density Functional Theory Analysis of Electronic and Optical Properties of Two-Dimensional Tantalum Carbides $Ta_{n+1}C_n$ (n = 1, 2, 3). *Phys. Status Solidi B Basic Solid State Phys.* **2019**, *256*, 1800457. [CrossRef]
23. Sun, D.; Hu, Q.; Chen, J.; Zhang, X.; Wang, L.; Wu, Q.; Zhou, A. Structural Transformation of MXene (V_2C, Cr_2C, and Ta_2C) with O Groups during Lithiation: A First-Principles Investigation. *ACS Appl. Mater. Interfaces* **2016**, *8*, 74–81. [CrossRef] [PubMed]
24. Wen, Y.; Rufford, T.E.; Chen, X.; Li, N.; Lyu, M.; Dai, L.; Wang, L. Nitrogen-doped $Ti_3C_2T_x$ MXene electrodes for high-performance supercapacitors. *Nano Energy* **2017**, *38*, 368–376. [CrossRef]
25. Zhou, J.; Zha, X.; Zhou, X.; Chen, F.; Gao, G.; Wang, S.; Shen, C.; Chen, T.; Zhi, C.; Eklund, P.; et al. Synthesis and Electrochemical Properties of Two-Dimensional Hafnium Carbide. *ACS Nano* **2017**, *11*, 3841–3850. [CrossRef] [PubMed]
26. Zhu, J.; Chroneos, A.; Eppinger, J.; Schwingenschlögl, U. S-functionalized MXenes as electrode materials for Li-ion batteries. *Appl. Mater. Today* **2016**, *5*, 19–24. [CrossRef]
27. Yadav, A.; Dashora, A.; Patel, N.; Miotello, A.; Press, M.; Kothari, D.C. Study of 2D MXene Cr_2C material for hydrogen storage using density functional theory. *Appl. Surf. Sci.* **2016**, *389*, 88–95. [CrossRef]
28. He, H.; Xia, Q.; Wang, B.; Wang, L.; Hu, Q.; Zhou, A. Two-dimensional vanadium carbide (V_2CT_x) MXene as supercapacitor electrode in seawater electrolyte. *Chin. Chem. Lett.* **2020**, *31*, 984–987. [CrossRef]
29. Wu, M.; Wang, B.; Hu, Q.; Wang, L.; Zhou, A. The Synthesis Process and Thermal Stability of V_2C MXene. *Materials* **2018**, *11*, 2112. [CrossRef]
30. Wu, M.; He, Y.; Wang, L.; Xia, Q.; Zhou, A. Synthesis and electrochemical properties of V_2C MXene by etching in opened/closed environments. *J. Adv. Ceram.* **2020**, *9*, 749–758. [CrossRef]
31. Rakhi, R.B.; Ahmed, B.; Anjum, D.; Alshareef, H.N. Direct Chemical Synthesis of MnO_2 Nanowhiskers on Transition-Metal Carbide Surfaces for Supercapacitor Applications. *ACS Appl. Mater. Interfaces* **2016**, *8*, 18806–18814. [CrossRef] [PubMed]
32. Xia, Q.X.; Shinde, N.M.; Yun, J.M.; Zhang, T.; Mane, R.S.; Mathur, S.; Kim, K.H. Bismuth Oxychloride/MXene symmetric supercapacitor with high volumetric energy density. *Electrochim. Acta* **2018**, *271*, 351–360. [CrossRef]
33. Yang, X.; Zhang, Y.; Fu, Z.; Lu, Z.; Zhang, X.; Wang, Y.; Yang, Z.; Wu, R. Tailoring the Electronic Structure of Transition Metals by the V_2C MXene Support: Excellent Oxygen Reduction Performance Triggered by Metal-Support Interactions. *ACS Appl. Mater. Interfaces* **2020**, *12*, 28206–28216. [CrossRef] [PubMed]
34. Le, T.A.; Tran, N.Q.; Hong, Y.; Lee, H. Intertwined Titanium Carbide MXene within a 3 D Tangled Polypyrrole Nanowires Matrix for Enhanced Supercapacitor Performances. *Chemistry* **2019**, *25*, 1037–1043. [CrossRef] [PubMed]
35. Zhou, Y.; Chen, L.; Jiao, Y.; Li, Z.; Gao, Y. Controllable fabrication of $ZnCo_2O_4$ ultra-thin curved sheets on Ni foam for high-performance asymmetric supercapacitors. *Electrochim. Acta* **2019**, *299*, 388–394. [CrossRef]
36. Sheberla, D.; Bachman, J.C.; Elias, J.S.; Sun, C.J.; Shao-Horn, Y.; Dinca, M. Conductive MOF electrodes for stable supercapacitors with high areal capacitance. *Nat. Mater* **2017**, *16*, 220–224. [CrossRef]
37. Yoon, Y.; Lee, M.; Kim, S.K.; Bae, G.; Song, W.; Myung, S.; Lim, J.; Lee, S.S.; Zyung, T.; An, K.-S. A Strategy for Synthesis of Carbon Nitride Induced Chemically Doped 2D MXene for High-Performance Supercapacitor Electrodes. *Adv. Energy Mater.* **2018**, *8*, 1703173. [CrossRef]
38. Zhang, X.; Shao, B.; Guo, A.; Sun, Z.; Zhao, J.; Cui, F.; Yang, X. MnO_2 nanoshells/$Ti_3C_2T_x$ MXene hybrid film as supercapacitor electrode. *Appl. Surf. Sci.* **2021**, *560*, 150040. [CrossRef]
39. Venkatkarthick, R.; Rodthongkum, N.; Zhang, X.; Wang, S.; Pattananuwat, P.; Zhao, Y.; Liu, R.; Qin, J. Vanadium-Based Oxide on Two-Dimensional Vanadium Carbide MXene ($V_2O_x@V_2CT_x$) as Cathode for Rechargeable Aqueous Zinc-Ion Batteries. *Acs Appl. Energy Mater.* **2020**, *3*, 4677–4689. [CrossRef]
40. Matthews, K.; Zhang, T.; Shuck, C.E.; VahidMohammadi, A.; Gogotsi, Y. Guidelines for Synthesis and Processing of Chemically Stable Two-Dimensional V_2CT_x MXene. *Chem. Mater.* **2021**, *34*, 499–509. [CrossRef]
41. VahidMohammadi, A.; Hadjikhani, A.; Shahbazmohamadi, S.; Beidaghi, M. Two-Dimensional Vanadium Carbide (MXene) as a High-Capacity Cathode Material for Rechargeable Aluminum Batteries. *ACS Nano* **2017**, *11*, 11135–11144. [CrossRef]
42. Guan, Y.; Jiang, S.; Cong, Y.; Wang, J.; Dong, Z.; Zhang, Q.; Yuan, G.; Li, Y.; Li, X. A hydrofluoric acid-free synthesis of 2D vanadium carbide (V_2C) MXene for supercapacitor electrodes. *2D Mater.* **2020**, *7*, 025010. [CrossRef]
43. Naguib, M.; Halim, J.; Lu, J.; Cook, K.M.; Hultman, L.; Gogotsi, Y.; Barsoum, M.W. New two-dimensional niobium and vanadium carbides as promising materials for Li-ion batteries. *J. Am. Chem. Soc.* **2013**, *135*, 15966–15969. [CrossRef]
44. Lin, H.; Wang, Y.; Gao, S.; Chen, Y.; Shi, J. Theranostic 2D Tantalum Carbide (MXene). *Adv. Mater.* **2018**, *30*, 1703284. [CrossRef]
45. Shan, Q.; Mu, X.; Alhabeb, M.; Shuck, C.E.; Pang, D.; Zhao, X.; Chu, X.-F.; Wei, Y.; Du, F.; Chen, G.; et al. Two-dimensional vanadium carbide (V_2C) MXene as electrode for supercapacitors with aqueous electrolytes. *Electrochem. Commun.* **2018**, *96*, 103–107. [CrossRef]
46. Dall'Agnese, Y.; Taberna, P.L.; Gogotsi, Y.; Simon, P. Two-Dimensional Vanadium Carbide (MXene) as Positive Electrode for Sodium-Ion Capacitors. *J. Phys. Chem. Lett.* **2015**, *6*, 2305–2309. [CrossRef] [PubMed]

47. VahidMohammadi, A.; Mojtabavi, M.; Caffrey, N.M.; Wanunu, M.; Beidaghi, M. Assembling 2D MXenes into Highly Stable Pseudocapacitive Electrodes with High Power and Energy Densities. *Adv. Mater.* **2019**, *31*, e1806931. [CrossRef]
48. Zhao, C.; Wang, Q.; Zhang, H.; Passerini, S.; Qian, X. Two-Dimensional Titanium Carbide/RGO Composite for High-Performance Supercapacitors. *ACS Appl. Mater. Interfaces* **2016**, *8*, 15661–15667. [CrossRef]